AIAA JOURNAL
Vol. 36, No. 4, April 1998

Probabilistic Structural Durability Prediction

Xiaoming Yu,* Kuang-Hua Chang,† and Kyung K. Choi‡
University of Iowa, Iowa City, Iowa 52242

An efficient reliability analysis method for durability of structural components subjected to external and inertial loads with time-dependent variable amplitudes is presented. This method is able to support reliability analysis of crack-initiation and crack-propagation lives of practical applications, considering uncertainties such as material properties, manufacturing tolerances, and initial crack size. Three techniques are employed to support the probabilistic durability prediction: 1) strain-based approach for multiaxial crack-initiation-life prediction and linear elastic fracture mechanics approach for crack-propagation-life prediction, 2) statistics-based approach for reliability analysis, and 3) sensitivity analysis and optimization methods for searching the most probable point (MPP) in the random variable space to compute the fatigue failure probability using the first-order reliability analysis method. A two-point approximation method is employed to speed up the MPP search. A tracked-vehicle roadarm is presented to demonstrate feasibility of the proposed method.

Nomenclature

$\boldsymbol{a}$	= transitional acceleration
a_c	= initial crack length
a_f	= finial (critical) crack length
$a_\Omega(z, \bar{z})$	= energy bilinear form
B	= strain-displacement matrix
b	= fatigue strength exponent
$\boldsymbol{b}$	= vector of design variables
c	= fatigue ductility exponent
D	= structural elasticity matrix
E	= structural Young's modulus
$\boldsymbol{F}_e(t)$	= vector of external-force history
$\boldsymbol{F}_i(t)$	= vector of inertial-force history
$f_1^a(\boldsymbol{x})$	= inertial body force per unit mass in translational direction
$f_1^r(\boldsymbol{x})$	= inertial body force per unit mass in radial direction
$f_i^t(\boldsymbol{x})$	= inertial body force per unit mass in the tangential direction
$f_i(\boldsymbol{x})$	= inertial body force per unit mass
$f_X(\boldsymbol{x})$	= joint probability density function of random vector $\boldsymbol{X}$
$g(\boldsymbol{X})$	= failure function
K	= stress intensity factor
$\mathcal{K}$	= stiffness matrix of structural component
K_c	= critical stress-intensity factor for fracture
$K_{\max}$	= maximum stress-intensity factor
$K_{\min}$	= minimum stress-intensity factor
$l_\Omega(\bar{z})$	= load linear form
N	= element shape function
N_f	= fatigue life to failure
N_0	= required fatigue life
P_f	= probability of failure
$\boldsymbol{q}^{\text{ine}}$	= equivalent nodal force of finite element model due to inertial force
$\boldsymbol{q}^k$	= unit force and torque applied at kth node
R	= ratio of maximum and minimum stress-intensity factors
$\boldsymbol{T}$	= transformation mapping
$\boldsymbol{T}(\boldsymbol{X}, \theta)$	= transformation from X space to a standard, uncorrelated normal U space
U	= random variable in U space
$\boldsymbol{U}$	= random vector in U space
U^*	= most probable point in U space
$\boldsymbol{V}$	= design velocity field
X	= random variable in X space
$\boldsymbol{X}$	= random vector in X space
X_1-X_2-X_3	= inertial frame of mechanical system
x'_{1_i}-x'_{2_i}-x'_{3_i}	= reference frame of the ith body
Z	= space of kinematically admissible virtual displacements
z	= vector of nodal displacement
$\bar{z}$	= virtual displacement
$\dot{z}$	= first-order material derivative of displacement vector
α	= angular acceleration
β	= reliability index
ΔK_{th}	= fatigue threshold stress-intensity factor
$\Delta \varepsilon/2$	= local uniaxial strain amplitude
$\Delta \varepsilon_{\text{eff}}/2$	= equivalent unixial strain-amplitude parameter
$\delta\boldsymbol{\sigma}_{\text{SIC}}$	= increment of stress-influence coefficient
ε	= true strain
ε_f	= fatigue ductility coefficient
ε^{LE}	= linear elastic local strain
μ_x	= mean value of a random variable X
ν_{eff}	= effective Poisson's ratio
$\rho(\boldsymbol{x})$	= mass density
σ	= true stress
$\boldsymbol{\sigma}^{\text{ext}}(t)$	= dynamic stress history due to external force
σ'_f	= fatigue strength coefficient
$\boldsymbol{\sigma}^{\text{ine}}(t)$	= dynamic stress history due to inertial force
$\boldsymbol{\sigma}_{\text{SIC}}$	= stress influence coefficient
$\boldsymbol{\sigma}_{\text{SIC}}^{\text{ine}}$	= stress influence coefficients due to inertial force
$\boldsymbol{\sigma}_{\text{SIC}}^k$	= stress influence coefficient due to unit force and torque applied at the kth node
σ^{LE}	= linear elastic local stress
$\boldsymbol{\sigma}(t)$	= dynamic stress history
σ_x	= standard deviation of a random variable X
Φ	= cumulative distribution function of standard normal function
ψ	= performance measure
Ω_e	= finite element domain
ω	= angular velocity

Presented as Paper 96-4063 at the AIAA/NASA/ISSMO 6th Symposium on Multidisciplinary Analysis and Optimization, Bellevue, WA, Sept. 4–6, 1996; received Sept. 27, 1997; revision received Oct. 31, 1997; accepted for publication Nov. 28, 1997.

*Research Assistant, Center for Computer-Aided Design; currently Technical Staff, Engineering Department, CSAR Corporation, 28035 Dorothy Drive, Agoura Hills, CA 91301. E-mail: xmy@whq.csar.com.

†Manager, CAE R&D, Center for Computer-Aided Design; currently Assistant Professor, School of Aerospace and Mechanical Engineering, University of Oklahoma, Norman, OK 73019. E-mail: khchang@ou.edu.

‡Professor and Director, Center for Computer-Aided Design and Department of Mechanical Engineering, College of Engineering. E-mail: kkchoi@ccad.uiowa.edu.

Introduction

STRUCTURAL fatigue from fluctuation of stresses generated over the service life of mechanical systems is the primary concern in structural design for durability and safety. Uncertainties in material properties, geometric dimensions due to manufacturing tolerances, and the type of environment to which the mechanical system is exposed constitute the indeterministic nature of the fatigue-life assessment for a structural component. A statistics-based approach that takes these uncertainties into account provides a more realistic and reliable assessment for structural durability and safety.

Early reliability analysis for fatigue life was based on the traditional stress–life method, which relates applied stresses directly to the total life.[1] This method is often used today, especially for high-cycle fatigue problems in which the notch strains are predominantly elastic. The stress–life method works well for designs involving long life and constant-amplitude loadings, such as power transmission shafts, springs, and gears. However, the stress–life method does not account for inelastic behavior and makes no distinction between crack initiation and propagation, and provides inadequate accuracy for low-cycle fatigue.[2] Moreover, because the damage parameter has no specific physical meaning in the stress–life method, this method cannot take into full account information on observed cracks or other measures of damages.[1]

Increasingly, reliability analysis for durability has focused on the fracture mechanics approach, i.e., probabilistic crack-propagation-life prediction, which describes the possibility of fatigue crack growth from an initial size to a critical size. The reason is that crack size can be used in fitness-for-purpose evaluations of damaged elements. Basically, there are two approaches for probabilistic crack-propagation-life prediction: predefined-straight-crack growth, and unknown-curved-crack growth.

A typical predefined-straight-crack-growth method is implemented in the probabilistic structural analysis computer program NESSUS (Numerical Evaluation of Stochastic Structures Under Stress).[3] Compared with a predefined-straight-crack path, the unknown-curved-crack path is more accurate. Besterfield et al.[4] developed a probabilistic finite element method for fatigue crack growth. They discretized the unknown crack path into many pieces of straight lines connected at each discretization point. The direction of these straight lines was determined by the crack direction law. Because the crack is modeled explicitly in the finite element model, the model is required to be remeshed and solved many times for each fatigue assessment. Consequently, this approach is very expensive for reliability analysis and has been demonstrated only for simple academic problems.

Compared with the probabilistic crack-propagation-life prediction, less research work has been done on probabilistic crack-initiation-life prediction. Prior research on probabilistic crack-initiation-life prediction is limited to simple cases in which constant-amplitude loads are considered and a simple crack-initiation theory is used, such as Ref. 5.

The Monte Carlo method has been employed extensively to calculate structural reliability. To reduce computational efforts in structural reliability analysis, many approximate techniques have been developed, such as the first-order reliability method (FORM), the second-order reliability method (SORM),[6] and the advanced mean value method (AMV+).[7] The critical step in the FORM or SORM and AMV+ is the most probable point (MPP) search. A widely used method for the MPP search is the Hasofer–Lind–Rackwitz–Fiessler (HL–RF) method.[6] Various MPP search methods have been reviewed.[7–9] Recently, the multipoint approximations have been developed by Wang and Grandhi[8,9] to support efficient MPP search.

The objective of this research is to develop an efficient reliability analysis method for fatigue crack-initiation and propagation lives of realistic structural components subjected to external and inertial loads with time-dependent variable amplitudes. In the proposed method, histories of dynamic stresses in the structural component are computed first using multibody dynamic analysis and finite element analysis (FEA). The strain–life approach is used to predict multiaxial crack initiation through a peak–valley editing of damage parameters and rainflow cycle-counting procedures. The dynamic stress history also is used to predict crack-propagation life using NASA/FLAGRO[10] to support propagation of various crack types. The FORM and AMV+ methods are employed to compute the reliability of crack-initiation and propagation lives of structural components, respectively. The two-point approximation (TPA)[11] method is used for the search of the MPP in the FORM. The sensitivity coefficients of crack-initiation and propagation lives with respect to random variables are calculated using the continuum design sensitivity analysis (DSA) method[12,13] to support the FORM and the AMV+.

The rest of the paper is organized as follows. Reliability analysis methods for the structural fatigue life using the FORM with TPA and the AMV+ are presented first. A structural fatigue life prediction method with emphasis on dynamic stress computation is discussed next. Then, the DSA method for the structural fatigue life is described. After discussing these methods, a tracked-vehicle roadarm is presented to demonstrate the proposed method. Conclusions are given in the final section of the paper.

Reliability Analysis Methods

To compute the reliability (or probability of failure) of a structure, a failure event corresponding to a structural performance measure, such as displacement, stress, buckling load factors, must be defined. For reliability analysis of structural fatigue life, the failure event or failure function is defined as

$$g(\boldsymbol{X}) = N_f(\boldsymbol{X}) - N_0 \tag{1}$$

where $N_f(\boldsymbol{X})$ is the structural fatigue life, i.e., number of cycles to fatigue, which is a function of random variables $\boldsymbol{X}$, and N_0 is the required fatigue life. When $N_f(\boldsymbol{X})$ is less than the required life N_0, that is, $g(\boldsymbol{X}) \leq 0$, the event fails. Therefore, the probability of failure P_f is defined as

$$P_f = P[g(\boldsymbol{X}) \leq 0] = P[N_f(\boldsymbol{X}) - N_0 \leq 0] \tag{2}$$

Given the joint probability density function $f_X(\boldsymbol{x})$ of the random variables $\boldsymbol{X}$, the probability of failure for a component-level reliability problem can be expressed as

$$P_f = P[g(\boldsymbol{X}) \leq 0] = \iint_{g(X) \leq 0} \dots \int f_X(\boldsymbol{x})\, \mathrm{d}\boldsymbol{x} \tag{3}$$

The multiple integral of Eq. (3) is very difficult to evaluate because the failure function is an implicit function of the random vector $\boldsymbol{X}$. Also, the multidimensional numerical integration over the failure region is extremely time-consuming. To overcome these difficulties, various methods, such as the Monte Carlo method, FORM, and SORM have been proposed. The Monte Carlo method provides a convenient, but time-consuming, solution for fatigue failure-probability prediction. On the other hand, FORM and SORM are much more efficient and are reasonably accurate.

FORM

To make use of properties of the standard normal space, a transformation is introduced to map the original random vector $\boldsymbol{X}$ to a standard, uncorrelated normal vector using $\boldsymbol{U} = \boldsymbol{T}(\boldsymbol{X})$, as shown in Fig. 1. If the random vector $\boldsymbol{X}$ is mutually independent with distribution functions f_{X_i}, $i = 1, 2, \dots, n$, the transformation is[1]

$$\boldsymbol{T}\colon U_i = \Phi^{-1}\big[f_{X_i}(\boldsymbol{x})\big], \qquad i = 1, 2, \dots, n \tag{4}$$

where $\Phi(\bullet)$ is the cumulative distribution function (CDF) of a normal distribution. If the random variables are not mutually independent, the Rosenblatt transformation[14] can be employed. Hasofer and Lind defined the reliability index as the shortest distance from the origin to a point on the failure surface in the U space.[6] Mathematically, it is a minimization problem with one equality constraint:

$$\beta = \min_{\boldsymbol{U}} |\boldsymbol{U}| \tag{5a}$$

subject to

$$g(\boldsymbol{U}) = 0 \tag{5b}$$

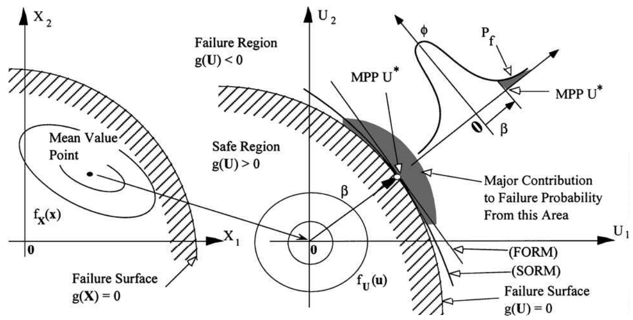

Fig. 1 Search of the MPP.

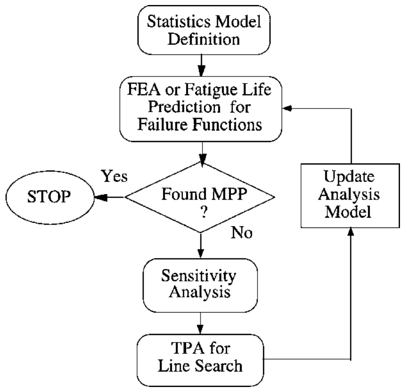

Fig. 2 Computation flow of the MPP search.

The solution U^* of the minimization problem is called the MPP or the design point. If the failure function $g(\boldsymbol{U})$ is linear in terms of the normally distributed random variables $\boldsymbol{U}$, the failure probability is[1]

$$P_f = P(g \leq 0) = \Phi(-\beta) \tag{6}$$

If the failure function is nonlinear or random variables are not normally distributed, a good approximation still can be obtained by using Eq. (6), provided that the magnitude of the principal curvatures of the failure surface at the MPP is not too large. Otherwise, the SORM must be used.

The computational flow of the MPP search is shown in Fig. 2, where the first-order derivatives of the structural failure function, such as the crack-initiation life, with respect to random variables, i.e., sensitivity analysis, are needed when searching for the MPP. The finite difference approach often is used for sensitivity analysis. This approach requires intensive computation of failure function evaluations for sensitivity analysis and often restricts the FORM to small-scale applications. Continuum DSA[12,13] offers an accurate and efficient alternative to sensitivity analysis of failure functions. This method allows computation of the sensitivity coefficients outside the established FEA codes by postprocessing FEA results.[15]

The MPP search is an important step of the FORM. A popular method of the MPP search is the HL–RF method.[6] Because the HL–RF method is inefficient or does not converge for highly nonlinear problems, various modifications have been proposed by introducing a line search. A TPA method[16] with proper move limits is adopted in this research to improve the efficiency and robustness of the HL–RF method.

MPP Search Using a TPA Method

The approximation method in structural optimization was introduced to reduce the number of FEA. This is accomplished by replacing the original optimization problem with a series of suboptimization problems that can be solved with less computation. Recently, Wang and Grandhi[8,9] applied the multipoint approximations to support efficient MPP search. Barthelemy and Haftka[17] reviewed recent advances in approximation concepts for optimal design, and pointed out that the TPA[16] was promising. In this paper, the TPA is used to improve efficiency and robustness of the HL–RF method. Using the TPA, intermediate variables y_i are introduced as

$$y_i = U_i^{p_i}, \qquad i = 1, 2, \ldots, n \tag{7}$$

where n is the number of random variables and P_i is the exponent for the ith random variable. Using the TPA, the approximation of the original reliability constraint (5b) is defined as

$$g(\boldsymbol{U})_{\mathrm{TPA}} = g\big(\boldsymbol{U}^{(k)}\big) + \sum_{i=1}^{n}\left[\left(\frac{U_i}{U_i^{(k)}}\right)^{p_i} - 1\right]\frac{U_i^{(k)}}{p_i}\frac{\partial g\big(\boldsymbol{U}^{(k)}\big)}{\partial U_i} = 0 \tag{8}$$

where k indicates the current iteration; $-\Delta\, U_i \leq U_i - U_i^{(k)} \leq \Delta\, U_i$, $i = 1, 2, \ldots, n$, where $\Delta\, U_i$ is a positive move limit used to improve robustness in optimization; and P_i is determined by

$$p_i = 1 + \left\{\left[\log\frac{\partial g\big(\boldsymbol{U}^{(k-1)}\big)}{\partial U_i} - \log\frac{\partial g\big(\boldsymbol{U}^{(k)}\big)}{\partial U_i}\right]\Big/ \left[\log\big(U_i^{(k-1)}\big) - \log\big(U_i^{(k)}\big)\right]\right\} \tag{9}$$

Numerical results show that TPA is more accurate than the linear approximation (LA) and the reciprocal approximation (RA) because more information is used to form the suboptimization problem.[16] The main advantage of TPA is its use of the exponent in P_i in the approximation equation (8), which is very versatile. If $P_i = 1$ for each random variable, TPA reduces to the LA; if $P_i = -1$, it reduces to the RA. Moreover, exponent P_i may be different for different random variables. These characteristics make the TPA capable of capturing the different behaviors of failure functions at various random variables. In fact, the dependency of structural failure functions on material properties, geometric parameters, and loadings could be quite different. Also, to prevent severe oscillation of the approximate failure function, the exponent P_i in Eq. (9) is restricted to be between -3 and 3. This explicit and nonlinear approximation problem can be solved by general-purpose optimization codes.

AMV+ Method

The FORM discussed earlier searches the MPP and approximates the failure probability P_f. On the other hand, the AMV method[7] establishes the CDF for given structural responses. The AMV iteration (AMV+) method[7] is developed to improve the accuracy of the AMV method. The AMV+ method is summarized briefly as follows. A detailed discussion can be found in Ref. 7.

The Taylor-series expansion of the structural fatigue life $N_f(\boldsymbol{X})$ at the mean values of random variables $\boldsymbol{X}$ can be expressed as

$$\begin{aligned} N_f(\boldsymbol{X}) &= N_f(\boldsymbol{\mu}) + \sum_{i=1}^{n}\frac{\partial N_f}{\partial X_i}(X_i - \mu_i) + H(\boldsymbol{X}) \\ &= a_0 + \sum_{i=1}^{n} a_i X_i + H(\boldsymbol{X}) \\ &= N_1(\boldsymbol{X}) + H(\boldsymbol{X}) \end{aligned} \tag{10}$$

where the derivatives a_i are evaluated at the mean values μ_i:

$$a_0 = N_f(\boldsymbol{\mu}) - \sum_{i=1}^{n}\frac{\partial N_f}{\partial X_i}\mu_i$$

is a constant, N_1 represents the sum of the first-order terms, and $H(\boldsymbol{X})$ represents the higher-order terms. Because N_1 is explicit and linear, its CDF can be computed efficiently.

Based on the AMV concept, two methods have been proposed to improve the CDF estimates: the specified CDF level method and the specified N_0 value method.[7] Both methods require iterations that involve evaluations and sensitivity analyses of the fatigue failure function until a convergent solution that is close to either the specified CDF level or the specified N_0 value is obtained.

Fatigue-Life Prediction

In structural durability analysis, structural fatigue life, including crack initiation and crack propagation, at critical points is calculated. The shortest life among these critical points is considered to be the fatigue life of the structural component. The computation of the structural fatigue life consists of two parts: dynamic-stress computation and fatigue-life computation. The dynamic stress can be obtained either from experiment (mounting sensors or transducers on a physical component) or from simulation. To carry out simulation,

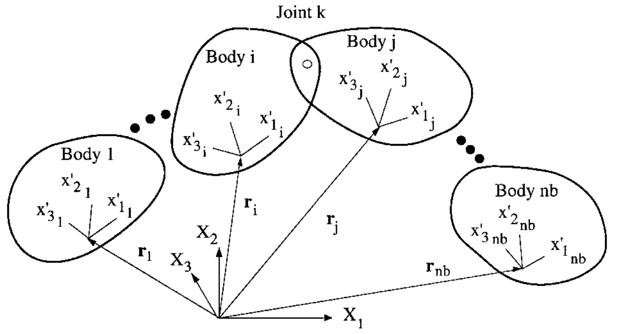

Fig. 3 Multibody mechanical system.

a number of quasistatic FEAs of the component are performed first. The stress influence coefficients (SICs) obtained from these quasistatic FEA then are superposed with the dynamic-analysis results, including external forces, accelerations, and angular velocities to compute dynamic stress history. Sanders and Tesar[18] show that the quasistatic deformation evaluation is a valid form of approximation for most industrial mechanisms that are stiff and operate substantially below their natural frequencies. Note that, in their work, they assume that deformation caused by applied external and inertial forces is small, compared with the geometry of the structural component. It is further assumed that the material from which the component is fabricated behaves in a linear elastic fashion. In this paper, the same assumptions are employed.

Multibody dynamic-analysis methods, which typically have been used for dynamic motion analysis, can be used for dynamic load analysis of mechanical systems,[19] e.g., a multibody system connected by joints as shown in Fig. 3. In this paper, all bodies of the dynamic model are assumed to be rigid. If the flexibility of bodies is large, such as the hull of a tracked vehicle, a flexible-body dynamic model must be employed. For suspension components of ground vehicles, the rigid-body assumption usually yields reasonably accurate analytical results to support structural design for durability.

The finite element model of the structural component corresponds to a specific body in the multibody dynamic model. It is desirable to create the finite element model on the body reference frame x'_{1_i}-x'_{2_i}-x'_{3_i} so that loadings, accelerations, and velocities generated from dynamic analysis that are calculated on the basis of body reference frame can be applied directly to the structural finite element model.

Because dynamic stress histories contain very large amounts of data, it is generally necessary to reduce or condense the amount of data by, for example, the peak–valley editing, before performing the crack-initiation-and crack-propagation-life computations.[20] These values then are used in a cycle-counting procedure to transform variable-amplitude stress or strain histories into a number of constant-amplitude stress or strain histories. These histories then are used to compute the crack-initiation life of the component. A multiaxial fatigue model using von Mises equivalent strain failure criteria is employed.[2]

The edited dynamic stress histories (without cycle counting) at the critical point also can be used for crack-propagation-life prediction. In this work, NASA/FLAGRO[10] is employed to support the crack-propagation-life computation. The FLAGRO takes edited dynamic stress histories as inputs to compute stress intensity factors, and then uses the stress intensity factors to calculate the crack-propagation life using approximation and empirical equations. The computation process for crack-initiation and crack-propagation life is illustrated in Fig. 4.

Dynamic Stress Computation

For the structural component subjected to external forces (joint reaction forces and torques) and inertial forces obtained from multibody dynamic analysis, the quasistatic equation in a matrix form of the finite element method can be written as

$$\boldsymbol{K}z = \boldsymbol{F}_e(t) - \boldsymbol{F}_i(t) \tag{11}$$

The dynamic stress then can be calculated using

$$\boldsymbol{\sigma}(t) = \boldsymbol{DBK}^{-1}[\boldsymbol{F}_e(t) - \boldsymbol{F}_i(t)] \tag{12}$$

where $\boldsymbol{D}$ is the material constitutive matrix.

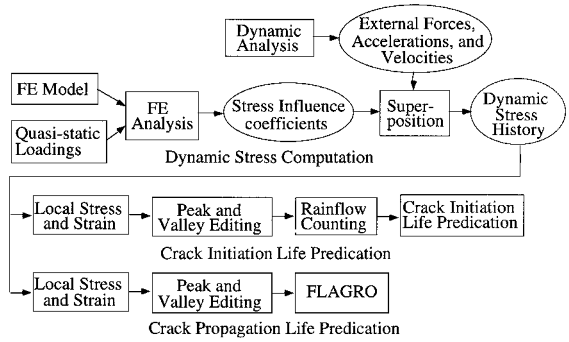

Fig. 4 Computation process for fatigue life.

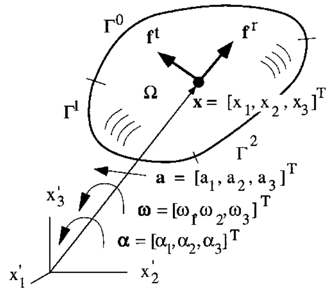

Fig. 5 Inertial forces applied to a component.

To use the quasistatic method with multibody dynamic analysis, the external forces and inertial forces acting on the component are separated into two parts: time-dependent (external- and inertial-force histories) and time-independent (quasistatic loading) forces. The quasistatic loading is treated as the static forces. The SICs are obtained by performing FEA for each quasistatic loading. The dynamic stresses then are calculated by using the superposition principle, that is, external- and inertial-force histories are multiplied by the corresponding SIC.

Quasistatic Loading for External Forces

A set of unit loads is used to calculate the SICs corresponding to joint reaction forces and torques. The unit loads are applied at a given point $\boldsymbol{x}$ in all degrees of freedom where joint reaction forces and torques act. For example, if a set of joint reaction forces and torques acts at the kth finite element node, the corresponding quasistatic loads $\boldsymbol{q}^k$ are three unit forces and three unit torques in the body reference frame of the jth body x'_{1_j}-x'_{2_j}-x'_{3_j} applied to the kth node as six loading cases. Therefore, the SIC $\boldsymbol{\sigma}^k_{\mathrm{SIC}}$ can be obtained using FEA:

$$\boldsymbol{\sigma}^k_{\mathrm{SIC}} = \boldsymbol{DBK}^{-1} q^k \tag{13}$$

Quasistatic Loading for Inertial Forces

The inertial body force applied to a point $\boldsymbol{x}$ of the component due to acceleration, angular velocity, and angular acceleration, as shown in Fig. 5, can be expressed as[21]

$$\begin{aligned} f_i(\boldsymbol{x}) &= f_i^a(\boldsymbol{x}) + f_i^r(\boldsymbol{x}) + f_i^t(\boldsymbol{x}) \\ &= -\rho(\boldsymbol{x})a_i - \rho(\boldsymbol{x})a_i^r + \rho(\boldsymbol{x})a_i^t \end{aligned} \tag{14}$$

where a_i is the instantaneous translational acceleration and is independent of the location of point $\boldsymbol{x}$, a_i^r is the centripetal acceleration toward the instantaneous axis of the rotation and is perpendicular to it, and a_i^t is the tangential acceleration. The radial and tangential accelerations $a_i^r(\boldsymbol{x})$ and $a_i^t(\boldsymbol{x})$ at point $\boldsymbol{x}$ can be written as

$$a_i^r(\boldsymbol{x}) = \omega_{ij}\omega_{jk}x_k \tag{15a}$$

and

$$a_i^t(\boldsymbol{x}) = \alpha_{ij}x_j \tag{15b}$$

where x_k is the kth coordinate of point $\boldsymbol{x}$, ω_{ij} is the instantaneous angular velocity, and α_{ij} is the instantaneous angular acceleration. The antisymmetric matrix notation that is formed from the component of a vector is employed for both $\boldsymbol{\omega}$ and $\boldsymbol{\alpha}$, i.e.,

$$\tilde{\boldsymbol{\omega}} \equiv \begin{bmatrix} 0 & -\omega_3 & \omega_2 \\ \omega_3 & 0 & -\omega_1 \\ -\omega_2 & \omega_1 & 0 \end{bmatrix} \equiv \begin{bmatrix} \omega_{11} & \omega_{12} & \omega_{13} \\ \omega_{21} & \omega_{22} & \omega_{23} \\ \omega_{31} & \omega_{32} & \omega_{33} \end{bmatrix} \tag{16a}$$

and

$$\tilde{\boldsymbol{\alpha}} \equiv \begin{bmatrix} 0 & -\alpha_3 & \alpha_2 \\ \alpha_3 & 0 & -\alpha_1 \\ -\alpha_2 & \alpha_1 & 0 \end{bmatrix} \equiv \begin{bmatrix} \alpha_{11} & \alpha_{12} & \alpha_{13} \\ \alpha_{21} & \alpha_{22} & \alpha_{23} \\ \alpha_{31} & \alpha_{32} & \alpha_{33} \end{bmatrix} \tag{16b}$$

Hence, the inertial body force at point $\boldsymbol{x}$ is

$$f_i(\boldsymbol{x}) = \rho(\boldsymbol{x})(-a_i - \alpha_{ij}x_j + \omega_{ij}\omega_{jk}x_k) \tag{17}$$

From the principle of virtual work, the load linear form due to inertia forces can be written as

$$l_\Omega(\bar{z}) = \iiint_\Omega f_i(\boldsymbol{x})\bar{z}_i \,\mathrm{d}\Omega \tag{18}$$

where Ω is the structural domain. For an element with diagonalized mass matrix, such as ANSYS,[22] the load linear form can be written as

$$l_\Omega(\bar{z}) = \left[-a_{il} + (-\alpha_{ij} + \omega_{ik}\omega_{kj})x_{jl}^n\right]m_{ll}^D \bar{z}_{mi}^n \tag{19}$$

where x_{lj}^n is the location of the element's lth node in the x_j direction; $\bar{z}_{mi}^n$ is the virtual displacement of the element's mth node in the x_i direction; and ρ is assumed to be constant. Also,

$$m_{ll}^D = m_{ll}(S/D)$$

where

$$S = \sum_{ij} m_{ij}, \qquad D = \sum_i m_{ii}$$

and m_{ij} is an entry of the consistent element mass matrix defined as

$$m_{ij} = \iiint_{\Omega_e} \rho N_i N_j \,\mathrm{d}\Omega_e$$

where N_i is an element shape function. Thus the load vector of a selected finite element is

$$\boldsymbol{q}_{i_e}^{\text{ine}} = \left[-a_{il} + (-\alpha_{ij} + \omega_{ik}\omega_{kj})x_{jl}^n\right]m_{ll}^D \tag{20}$$

where the subscript e indicates that the load vector $\boldsymbol{q}_{i_e}^{\text{ine}}$ is obtained at the finite element level.

It can be seen from Eq. (20) that the inertial force $\boldsymbol{q}$ is linearly dependent on components of the acceleration $\boldsymbol{a}$ and the angular acceleration $\boldsymbol{\alpha}$. However, the inertial force is not linearly dependent on components of the angular velocities $\boldsymbol{\omega}$. Instead, it depends linearly on the combinations of components of the angular velocities $\boldsymbol{\omega}$, such as $\omega_1\omega_2$.

Note that the SIC of the first six quasistatic loads can be obtained by applying unit accelerations [instead of evaluating Eq. (20)] and performing FEA, using established FEA codes. However, Eq. (20) must be evaluated to obtain the equivalent nodal forces corresponding to the last six quasistatic loads involving the angular velocities, which can be applied to the finite element model as external nodal forces. The SIC $\boldsymbol{\sigma}_{\text{SIC}}^{\text{ine}}$ due to inertial forces can be obtained using FEA, as

$$\boldsymbol{\sigma}_{\text{SIC}_l}^{\text{ine}} = \boldsymbol{DBK}^{-1}\boldsymbol{q}_l^{\text{ine}}, \qquad l = 1, \ldots, 12 \tag{21}$$

where $\boldsymbol{q}_l^{\text{ine}} = [q_i^{\text{ine}}]_l$ and q_i^{ine} is the summation of Eq. (20) over all finite elements in the structural component.

Dynamic Stress Computation

The dynamic stress is calculated using the superposition principle as

$$\boldsymbol{\sigma}(t) = \boldsymbol{\sigma}^{\text{ine}}(t) + \boldsymbol{\sigma}^{\text{ext}}(t) \tag{22}$$

where

$$\begin{aligned} \boldsymbol{\sigma}^{\text{ine}}(t) &= \sum_{l=1}^{3} \boldsymbol{\sigma}_{\text{SIC}_l}^{\text{ine}} a_l(t) + \sum_{l=1}^{3} \boldsymbol{\sigma}_{\text{SIC}_{(l+3)}}^{\text{ine}} \alpha_l(t) + \boldsymbol{\sigma}_{\text{SIC}_7}^{\text{ine}} \omega_1(t)\omega_2(t) \\ &+ \boldsymbol{\sigma}_{\text{SIC}_8}^{\text{ine}} \omega_2(t)\omega_3(t) + \boldsymbol{\sigma}_{\text{SIC}_9}^{\text{ine}} \omega_1(t)\omega_3(t) + \boldsymbol{\sigma}_{\text{SIC}_{10}}^{\text{ine}}\left[\omega_2^2(t) + \omega_3^2(t)\right] \\ &+ \boldsymbol{\sigma}_{\text{SIC}_{11}}^{\text{ine}}\left[\omega_1^2(t) + \omega_3^2(t)\right] + \boldsymbol{\sigma}_{\text{SIC}_{12}}^{\text{ine}}\left[\omega_1^2(t) + \omega_2^2(t)\right] \end{aligned} \tag{23}$$

in which $\boldsymbol{\sigma}_{\text{SIC}_l}^{\text{ine}}$ is obtained from Eq. (21). Also,

$$\boldsymbol{\sigma}^{\text{ext}}(t) = \sum_{k=1}^{n} \boldsymbol{\sigma}_{\text{SIC}}^k \boldsymbol{F}^k(t) \tag{24}$$

where $\boldsymbol{\sigma}_{\text{SIC}}^k$ can be obtained from Eq. (13) and n is the number of nodes to which external forces $\boldsymbol{F}^k(t)$ are applied.

Because most cracks are initiated at the structural surface, and the stress computed using displacement-based FEA at the surface is usually less accurate, a stress smoothing technique that uses the least-squares method[21] is employed in this work to improve accuracy of the stress at the surface.

Multiaxial Crack-Initiation-Life Prediction

Strain-based fatigue crack initiation models[23] are employed. A number of life prediction methods, such as von Mises equivalent strain,[23,24] the American Society of Mechanical Engineers (ASME) Boiler Code,[23,25] and the tensile and shear critical plane,[23,26] are commonly used and have been implemented in the DRAW[20] (Durability and Reliability Analysis Workspace) tool. Strain-based fatigue crack-initiation-life prediction models attempt to correlate a known local elastic–plastic strain state from a specimen or structural component to the crack-initiation life of the specimen or component. The fatigue crack-initiation life is usually considered to be the number of loading cycles or history blocks necessary to form a microcrack, usually a detectable surface crack of a length of 0.25–2.5 mm, although no standard definition exists.

Local Strain Approach

Uniaxial low-cycle fatigue models,[27] that is, the local strain approach, have become the most popular means of predicting crack-initiation life of structural components subject to uniaxial loading. Fatigue resistance of material can be characterized by a strain-life curve such as the one shown in Fig. 6. This curve is determined from polished laboratory specimens tested under a completely reversed strain control.

In accordance with the strain-life curve, the low-cycle fatigue strain-life relation is given as

$$\Delta\,\varepsilon/2 = (\sigma_f'/E)(2N_f)^b + \varepsilon_f'(2N_f)^c \tag{25}$$

where $2N_f$ is fatigue crack-initiation life. Modifications to this equation have been proposed to account for mean stress effects, for example, Morrow and Smith–Watson–Topper mean stress models.[23]

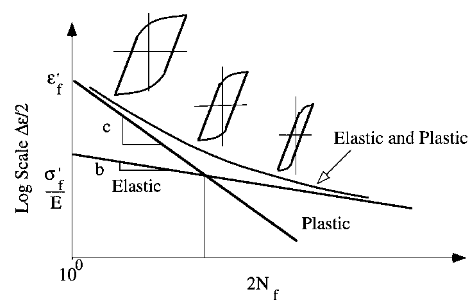

Fig. 6 Strain-life curve.

Given a uniaxial, variable-amplitude local strain-time history, a peak–valley editing routine[28] followed by a rainflow counting routine[23] will produce a series of defined local strain cycles. Using the amplitude $\Delta\,\varepsilon/2$ of each of these defined local strains in Eq. (25), the corresponding fatigue life for each defined cycle can be determined. Using an appropriate damage summation rule, the individual fatigue life of these defined cycles can be combined to obtain the predicted fatigue crack-initiation life for the given local strain-time history. An HMMWV (High Mobility Multipurpose Wheeled Vehicle) lower control arm was tested using a material testing system to validate the fatigue-life computation method.[29] The result shows a 20–50% difference between the computation and the actual test.

Multiaxial Fatigue Models

In most structural components, stress/strain fields are multiaxial. The main task in extending the local strain approach to a multiaxial loading situation is to propose an appropriate strain-based damage parameter, analogous to the uniaxial strain amplitude $\Delta\,\varepsilon/2$ in Eq. (25), with which to correlate the fatigue crack-initiation life of a structural component subjected to a multiaxial loading. In general, there are three different approaches for fatigue crack-initiation-life prediction under multiaxial loading: equivalent stress/strain (e.g., von Mises equivalent strain, ASME Boiler Code, and tensile and shear critical plane), energy-based, and critical plane.[23] In this research, the equivalent stress/strain approach is employed, and the von Mises equivalent strain is illustrated further.

Based on the definition of an equivalent-stress parameter proposed by the von Mises yield criterion, this approach defines the equivalent uniaxial strain amplitude parameter $\Delta\,\varepsilon_{\mathrm{eff}}/2$ as

$$\frac{\Delta\,\varepsilon_{\mathrm{eff}}}{2} = \frac{1}{\sqrt{2(1+\nu_{\mathrm{eff}})}}\left\{\left(\frac{\Delta\,\varepsilon_{11}}{2}-\frac{\Delta\,\varepsilon_{22}}{2}\right)^2+\left(\frac{\Delta\,\varepsilon_{22}}{2}-\frac{\Delta\,\varepsilon_{33}}{2}\right)^2 + \left(\frac{\Delta\,\varepsilon_{33}}{2}-\frac{\Delta\,\varepsilon_{11}}{2}\right)^2+6\left(\frac{\Delta\,\varepsilon_{12}}{2}+\frac{\Delta\,\varepsilon_{13}}{2}+\frac{\Delta\,\varepsilon_{23}}{2}\right)^2\right\}^{\frac{1}{2}} \tag{26}$$

where ν_{eff} is the effective Poisson's ratio defined as

$$\nu_{\mathrm{eff}} = 0.5 - (0.5-\nu)(E_{\mathrm{eff}}/E) \tag{27}$$

where E_{eff} is the effective secant modulus.[26]

Crack-Propagation-Life Prediction

The driving force for extension of a crack is not the strain or stress but the stress intensity factor K. The NASA/FLAGRO computer program is employed to predict crack-propagation life. FLAGRO takes edited dynamic stress histories as inputs to compute stress intensity factors, and then uses these factors to calculate crack-propagation life for a given initial crack, a predefined final crack size, and an assumed crack shape. In FLAGRO, stress intensity factors are approximated using a simple formulation.

The crack-growth-rate equation incorporated into the NASA/FLAGRO is the modified Forman's equation, expressed as[30]

$$\frac{\mathrm{d}a}{\mathrm{d}N_f} = f(\Delta\,K) = \frac{C(1-R)^m\Delta\,K^n(\Delta\,K-\Delta\,K_{\mathrm{th}})^p}{[(1-R)K_c-\Delta\,K]^q} \tag{28}$$

where R is the ratio of maximum and minimum stress intensity factors, i.e., $K_{\max}/K_{\min}$, K_c is the critical stress intensity factor for fracture; $\Delta\,K_{\mathrm{th}}$ is the fatigue threshold stress intensity factor range; and m, n, p, and q are the exponents of a modified Forman equation.

The crack growth life, in terms of cycles to failure, can be calculated using Eq. (28). Thus, cycles to failure, N_f, can be calculated as

$$N_f = \int_{a_c}^{a_f}\frac{\mathrm{d}a}{f(\Delta\,K)} \tag{29}$$

where a_c is the initial crack length and a_f is the preset finial (critical) crack length. The fatigue crack-growth prediction module calculates the crack extension $\mathrm{d}a$ in each cycle of a sequence of cycles and adds it to the current crack size. This process proceeds until the failure condition is reached or a preset crack size is achieved. In each cycle, the apparent or applied $\Delta\,K$ is calculated from the stress range that is obtained from dynamic stress computation for uncracked structures, the crack size, and the built-in NASA/FLAGRO geometry of the component under consideration. The $\Delta\,K$ computation is very efficient because the crack is not explicitly modeled or grown in the finite element model. In addition, the intensive dynamic stress computation is needed only once for fatigue-life assessment. For more accurate $\Delta\,K$ computations, a number of advanced techniques, such as crack elements, mixed-mode crack propagation criteria, and automatic remeshing, must be employed.[31] In general, this computation is very time-consuming because the dynamic stress computation will be repeated several times for each fatigue-life assessment. Note that the error in $\Delta\,K$ obtained using a less accurate but efficient approach is small compared to uncertainties in a fatigue analysis, such as material properties and the load history.[23]

If the crack closure occurs at a level that is above $K_{\min}$ in the cycle, the crack growth rate will be reduced, as the driving force that the crack tip experiences is reduced. The crack closure analysis that calculates the effect of R on crack growth rate under the constant amplitude loading is used in this work. Based on Newman's equation, it is expressed in the form

$$\Delta\,K_2 = \left[\frac{1-(S_0/S_{\max})_1}{1-(S_0/S_{\max})_2}\,\frac{1-R_1}{1-R_2}\right]\Delta\,K_1 \tag{30}$$

where $\Delta\,K_1$ is a baseline or known $\Delta\,K$ value corresponding to a $\mathrm{d}a/\mathrm{d}N$ for $R = R_1$ ($R_1 = 0$); $\Delta\,K_2$ is the $\Delta\,K$ value that gives the same $\mathrm{d}a/\mathrm{d}N$ at a different R value, i.e., R_2; S_0 is the crack opening stress; and $S_{\max}$ is the maximum cyclic stress. More detailed procedures can be found in Ref. 30.

Sensitivity Analysis for Fatigue Lives

If the FORM is used to solve the reliability of the structural fatigue life, the sensitivity coefficients of the fatigue life with respect to random variables are necessary for the MPP search. Methods of the sensitivity computation have significantly affected the efficiency of reliability analysis. Note that the dynamic stress computation dominates the CPU time for durability analysis.[21] Once dynamic stresses are obtained, the crack-initiation and propagation-life calculation is very efficient compared to the dynamic stress computation time. Thus, for random variables that do not affect dynamic stresses, e.g., fatigue material properties, a finite difference method is very efficient for the sensitivity calculation. For random variables that affect dynamic stresses, e.g., structural dimensions, the hybrid DSA method[21] is employed because, in this case, the fatigue life cannot be expressed as a function of random variables due to the peak–valley editing and cycle counting procedures. The computation procedure of the hybrid DSA method is illustrated in Fig. 7.

Shape Sensitivity Analysis for Stress Measures

In continuum-shape DSA, parameters that determine the geometric shape of the structural domain are treated as design parameters. The relationship between the shape variation of a continuous domain and the resulting variation in the structural performance measure can be described using the material derivative idea in continuum

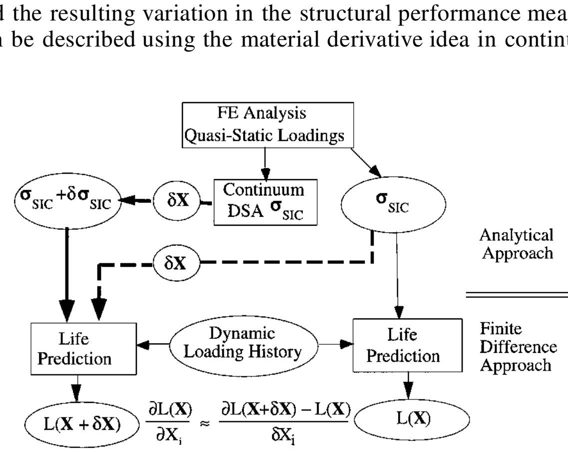

Fig. 7 Hybrid DSA for fatigue life: ——, stress-dependent random variables, and – – –, stress-independent random variables.

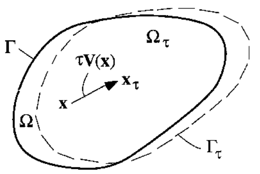

Fig. 8 Deformation process.

mechanics. A general shape sensitivity expression and the velocity field are introduced first. The DSA expression then is applied to three-dimensional solids with inertial forces.

Design Velocity Field

Consider the structural domain as a continuous medium, and the process of changing the shape of domain Ω to Ω_τ in Fig. 8 as a dynamic process that deforms the continuum with τ playing the role of time. The transformation mapping $\boldsymbol{T}$ that represents this process can be defined as[12,13]

$$\boldsymbol{T}: \boldsymbol{x} \to \boldsymbol{x}(\boldsymbol{x}), \qquad \boldsymbol{x} \in \Omega_\tau \tag{31}$$

where

$$\left.\begin{aligned} \boldsymbol{x}_\tau &\equiv \boldsymbol{T}(\boldsymbol{x}, \tau) \\ \Omega_\tau &\equiv \boldsymbol{T}(\Omega, \tau) \\ \Gamma_\tau &\equiv \boldsymbol{T}(\Gamma, \tau) \end{aligned}\right\} \tag{32}$$

Suppose that a material point $\boldsymbol{x} \in \Omega$ in the initial domain at $\tau = 0$ moves to a new location $\boldsymbol{x}_\tau \in \Omega_\tau$ in the perturbed domain. Then, the velocity field $\boldsymbol{V}$ can be defined as

$$\boldsymbol{V}(\boldsymbol{x}_\tau, \tau) \equiv \frac{\mathrm{d}x_\tau}{\mathrm{d}\tau} = \frac{\mathrm{d}\boldsymbol{T}(\boldsymbol{x}, \tau)}{\mathrm{d}\tau} = \frac{\partial \boldsymbol{T}(\boldsymbol{x}, \tau)}{\partial \tau} \tag{33}$$

In the neighborhood of initial time $\tau = 0$, assuming a regularity hypothesis and ignoring higher-order terms, T can be approximated by

$$\begin{aligned} \boldsymbol{T}(\boldsymbol{x}, \tau) &= \boldsymbol{T}(\boldsymbol{x}, 0) + \tau \frac{\partial \boldsymbol{T}(\boldsymbol{x}, 0)}{\partial \tau} + \mathcal{O}(\tau^2) \\ &\approx \boldsymbol{x} + \tau \boldsymbol{V}(\boldsymbol{x}, 0) \end{aligned} \tag{34}$$

where $\boldsymbol{x} \equiv \boldsymbol{T}(\boldsymbol{x}, 0)$ and $\boldsymbol{V}(\boldsymbol{x}) \equiv \boldsymbol{V}(\boldsymbol{x}, 0)$.

Shape Sensitivity Analysis

A variational governing equation for a structural component with the domain Ω can be written as

$$a_\Omega(z, \bar{z}) = l_\Omega(\bar{z}), \qquad \text{for all} \quad \bar{z} \in Z \tag{35}$$

The subscript Ω in Eq. (35) is used to indicate the dependency of the governing equation on geometric shape of the structural domain.

A general performance measure that depends on the displacement and stress can be written in an integral form as

$$\psi = \iint_\Omega g(z, \nabla z)\, \mathrm{d}\Omega \tag{36}$$

Using the adjoint variable method of shape DSA,[12,13] the variation of the performance measure ψ of Eq. (36) can be expressed as

$$\begin{aligned} \psi' = l'_V(\boldsymbol{\lambda}) - a'_V(z, \boldsymbol{\lambda}) - \iint_\Omega \big[g_{,z}\big(\nabla z^T \boldsymbol{V}\big) \\ + g_{,\nabla z} \nabla(\nabla z^T \boldsymbol{V})\big]\, \mathrm{d}\Omega + \int_\Gamma g(\boldsymbol{V}^T \boldsymbol{n})\, \mathrm{d}\Gamma \end{aligned} \tag{37}$$

where $\boldsymbol{\lambda}$ is the solution of the adjoint equation

$$a_\Omega(\boldsymbol{\lambda}, \bar{\boldsymbol{\lambda}}) = \iint_\Omega \big[g_{,z}\bar{\boldsymbol{\lambda}} + g_{,\nabla z}\nabla\bar{\boldsymbol{\lambda}}\big]\, \mathrm{d}\Omega, \qquad \text{for all } \bar{\boldsymbol{\lambda}} \in Z \tag{38}$$

Using the direct differentiation method, the first variation of the performance measure ψ can be written as

$$\begin{aligned} \psi' = \iint_\Omega \big[g_{,z}\dot{z} + g_{,\nabla z}\nabla\dot{z} - g_{,z}(\nabla z^T \boldsymbol{V}) - g_{,\nabla z}\nabla(\nabla z^T \boldsymbol{V})\big]\, \mathrm{d}\Omega \\ + \int_\Gamma g(\boldsymbol{V}^T \boldsymbol{n})\, \mathrm{d}\Gamma \end{aligned} \tag{39}$$

where $\dot{z}$ is the solution of the sensitivity equation obtained by taking the material derivative of Eq. (35), i.e.,

$$a_\Omega(\dot{z}, \bar{z}) = l'_V(\bar{z}) - a'_V(z, \bar{z}), \qquad \text{for all } \bar{z} \in Z \tag{40}$$

The subscript $\boldsymbol{V}$ on the right-hand side of Eqs. (37), (39), and (40) is used to indicate the dependency of the terms on the velocity field.[32]

Numerical evaluation of Eqs. (37) and (39) requires knowledge of the original structural response z, adjoint response $\boldsymbol{\lambda}$ or material derivative $\dot{z}$, and the velocity field $\boldsymbol{V}$. Structural responses z, $\boldsymbol{\lambda}$, and $\dot{z}$ can be obtained following rather routine computations. However, the velocity field $\boldsymbol{V}$ must be computed carefully so that it satisfies theoretical and practical requirements.[32]

Variation of Load Linear Form

With no traction force at the design boundary, a variation of the load linear form of Eq. (35) can be written as[12,13]

$$l'_V(\bar{z}) = \iiint_\Omega [f'_i \bar{z}_i + \bar{z}_i(f_{i,j}V_j) + f_i\bar{z}_i \operatorname{div} \boldsymbol{V}]\, \mathrm{d}\Omega + \dot{q}_i\bar{z}_i \tag{41}$$

where

$$f'_i \equiv \lim_{\tau \to 0} \frac{f_{i_\tau}(x) - f_i(x)}{\tau} = 0 \tag{42}$$

and $f_{i_\tau}(\boldsymbol{x}) = f_i(\boldsymbol{x})$ because the inertial force evaluated at a fixed material point $\boldsymbol{x}$ before and after design changes is constant. Note that the variation of $q_i\bar{z}_i$ is zero because q_i (corresponding to a joint reaction force) is assumed to be independent of design changes. Therefore, $\dot{q}_i = 0$ for the quasistatic load corresponding to the joint reaction force. The variation of the quasistatic load linear form corresponding to inertial forces can be written as[21]

$$l'_V(\bar{z}) = \big[(-\alpha_{ij} + \omega_{ik}\omega_{kj})\big(V^n_{jl}m_{lm} + x^n_{jl}\dot{m}^D_{ll}\big) - a_i\dot{m}^D_{ll}\big]\bar{z}^n_{li} \tag{43}$$

for a finite element with a diagonalized mass matrix, where

$$\dot{m}^D_{ll} = \dot{m}_{ll}(S/D) + m_{ll}(\dot{S}/D) - \dot{m}_{ll}(S/D^2)\dot{D} \tag{44}$$

and

$$\dot{S} = \sum_{ij} \dot{m}_{ij}, \qquad \dot{D} = \sum_i \dot{m}_{ii}$$

and

$$\dot{m}_{ij} = \rho \iiint_\Omega N_l N_m \operatorname{div} V\, \mathrm{d}\Omega$$

Design Sensitivity of Fatigue Life

As shown in Fig. 7, the finite difference method is used to compute the sensitivity of the component fatigue life. Once the sensitivities of the SIC are obtained using the continuum DSA method described earlier, the increment of the SIC can be obtained by

$$\delta\boldsymbol{\sigma}_{\mathrm{SIC}} = \frac{\partial \boldsymbol{\sigma}_{\mathrm{SIC}}}{\partial X_j}\delta X_j \tag{45}$$

where δX_j is the perturbation of the jth random variable. Note that the perturbation δX_j must be small for linear approximation of the fatigue life. On the other hand, in numerical calculation, δX_j cannot be too small because it introduces numerical noise.

The SIC of the perturbed model can be approximated by

$$\boldsymbol{\sigma}_{\mathrm{SIC}}(\boldsymbol{X} + \delta X_j) \approx \boldsymbol{\sigma}_{\mathrm{SIC}}(\boldsymbol{X}) + \delta\boldsymbol{\sigma}_{\mathrm{SIC}} \tag{46}$$

A stress time history of the perturbed model can be obtained by superposing $\boldsymbol{\sigma}_{\mathrm{SIC}}(\boldsymbol{X} + \delta X_j)$ with the same loading history obtained from multibody dynamic analysis. Note that the perturbation is assumed to be local so that the dynamic behavior of the mechanical system is not altered. The new dynamic stress history then is used to calculate the fatigue life of the structural component with a perturbed random variable, $L(X + \delta X_j)$, using the same life prediction method. The sensitivity coefficient of component fatigue life with respect to the jth random variable can be obtained from

$$\frac{\partial L}{\partial X_j} \approx \frac{L(X + \delta X_j) - L(X)}{\delta X_j} \tag{47}$$

Note that Eqs. (45–47) must be evaluated repeatedly for all random variables that affect dynamic stresses. This computation is very efficient because the sensitivities of the SIC are available.[21]

Numerical Example

A roadarm of the military tracked vehicle shown in Fig. 9 is employed to demonstrate the proposed method for probabilistic fatigue-life prediction. First, the multibody dynamic model of the tracked vehicle and its simulation environment are described. The structural finite element model of the roadarm then is discussed. A deterministic fatigue-life prediction of the roadarm is discussed next. Definition of random variables and probabilistic fatigue-life predictions of the roadarm are presented as final results.

Multibody Dynamic Model and Simulation

A 17-body dynamics model shown in Fig. 10 is generated to drive the tracked vehicle on the Aberdeen Proving Ground 4 (APG4), at a constant speed of 20 mph forward (positive X_2 direction). A 20-s dynamic simulation is performed at a maximum integration time step of 0.05 s using DADS.[33] The joint reaction forces applied at the wheel end of the roadarm, accelerations, angular velocities, and angular accelerations of the roadarm are obtained from the analysis.

Roadarm Finite Element Model

Four beam elements (STIF4) and 310 20-node isoparametric finite elements (STIF95) of ANSYS are used for the roadarm finite element model, as shown in Fig. 11. The roadarm is made of S4340 steel, with material properties of Young's modulus $E = 3.0 \times 10^7$ psi and Poisson's ratio $\nu = 0.3$. The coordinate system of the finite element model is selected to be identical to the body reference frame of the roadarm in the tracked-vehicle dynamic model. Therefore, the loading history generated from dynamic analysis can be used without transformation.

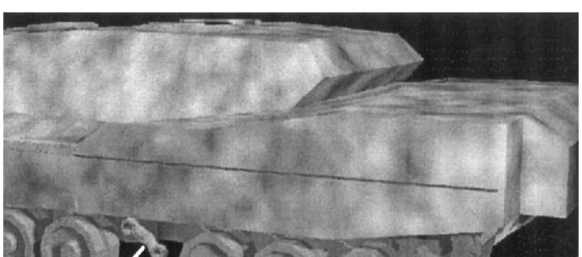

Fig. 9 Military tracked vehicle and roadarm.

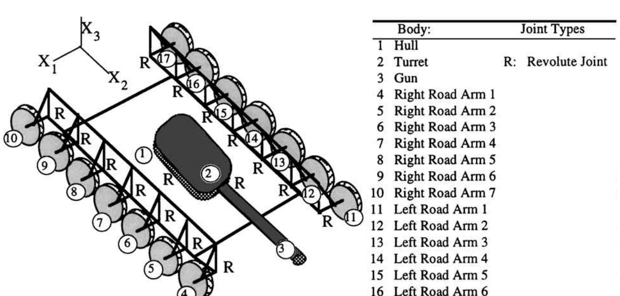

Fig. 10 Tracked-vehicle dynamic model.

Table 1 Definition of random variables for crack-initiation-life prediction

Random variables	Mean value	Standard deviation	Distribution
Young's Modulus E	30.0E+6	0.75E+6	Log normal
Fatigue strength coefficient σ_f'	1.77E+5	0.885E+4	Log normal
Fatigue ductility coefficient ε_f'	0.41	0.0205	Log normal
Fatigue strength exponent b	−0.07300	0.00365	Normal
Fatigue ductility exponent c	−0.6	0.003	Normal
Tolerance $b1$	3.2496	0.032450	Normal
Tolerance $b2$	1.9675	0.019675	Normal
Tolerance $b3$	3.1703	0.031703	Normal
Tolerance $b4$	1.9675	0.019675	Normal
Tolerance $b5$	3.1703	0.031703	Normal
Tolerance $b6$	2.6352	0.026352	Normal
Tolerance $b7$	3.2496	0.032496	Normal
Tolerance $b8$	5.0568	0.050568	Normal

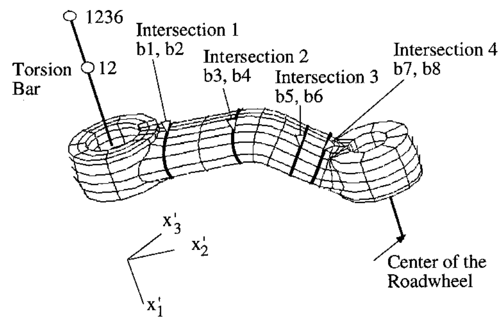

Fig. 11 Roadarm finite element model.

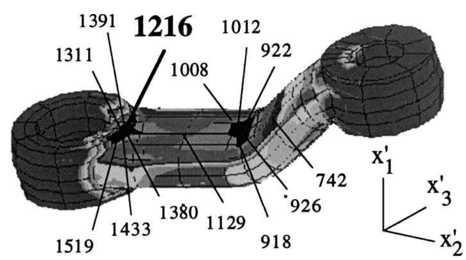

Fig. 12 Contour of crack-initiation life.

Deterministic Crack-Initiation-Life Prediction

FEA is performed first to obtain the SIC of the roadarm using ANSYS by applying 18 quasistatic loads. Among these loads, the first six that correspond to external joint forces are three unit forces and three unit torques applied at the center of the roadwheel, in x_1', x_2', and x_3' directions, and the remaining 12 quasistatic loads that correspond to inertial forces are unit accelerations, unit angular accelerations, and unit combinations of angular velocities.

The dynamic stresses at finite element nodes then are calculated by superposing SIC with their corresponding external forces and accelerations and velocities in a time domain obtained from the dynamic simulation. To compute multiaxial crack-initiation life of the roadarm, the equivalent von Mises strain approach[20] is employed. The fatigue-life contour is given in Fig. 12. The total computation for fatigue-life prediction took 7084 CPU seconds on an HP 9000/750.

Probabilistic Fatigue-Life Predictions

The random variables and their statistical values for the crack-initiation-life prediction are listed in Table 1, including the material and tolerance random variables. The eight tolerance random variables are defined to characterize the four cross-sectional shapes of the roadarm. Contour of the cross-sectional shape is composed of four straight lines and four cubic curves as shown in Fig. 13. Side variations (x_2' direction) of cross-sectional shapes are defined as random variables $b1$, $b3$, $b5$, and $b7$ for intersections 1–4, respectively

Table 2 Definition of random variables for crack-propagation-life prediction

Random variables	Mean value	Standard deviation	Distribution
Initial crack length a_c	0.025	0.0125	Normal
Yielded stress σ_{ys}	180.0	36.0	Log normal
Fracture toughness K_{IC}	90.0	18.0	Log normal
Forman coefficient C	0.791E−08	0.2373E−08	Normal
Forman exponent n	1.984	0.3968	Normal
Forman exponent p	0.25	0.0125	Normal
Forman exponent q	0.25	0.0125	Normal
Fitting parameter ΔK_0	4.0	0.2	Normal
Fitting parameter C_0	1.0	0.05	Normal
Fitting parameter d	0.5	0.025	Normal

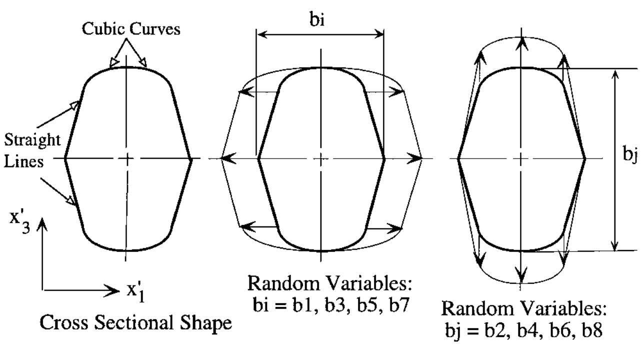

Fig. 13 Tolerance random variable definition.

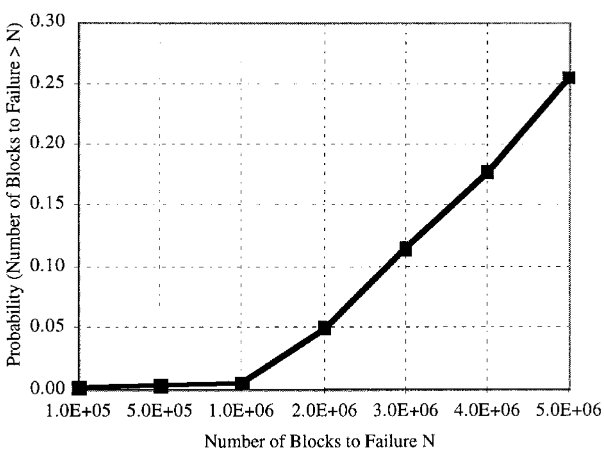

Fig. 14 CDF of failure of crack-initiation life.

(see Fig. 11). Vertical variations (x_3' direction) of the cross-sectional shapes are defined using the remaining four random variables, as shown in Fig. 13.

The FORM with TPA is used to calculate the reliability of the crack-initiation life. The deterministic fatigue life at node 1216 is the shortest with 9.63E+06 blocks (20 s per block). The CDF of the crack-initiation life (number of blocks to failure) at node 1216 is shown in Fig. 14. The horizontal axis in Fig. 14 is the required number of service blocks, and the vertical axis is the failure probability. The CDF in Fig. 14 is obtained by carrying out reliability analysis at the seven required numbers of service blocks, which are marked in Fig. 14.

Note that one FORM is equivalent to a deterministic optimization. For the roadarm example, each reliability analysis took three fatigue-life computations and three fatigue DSAs. The total computation time is 10 CPU hours on an HP 9000/750. In actual design applications, the CDF curve can be used to obtain the failure probability for the required number of service blocks before crack initiation, or a required number of service blocks before crack initiation with a required reliability. For example, it can be seen from Fig. 14 that, if the required number of service blocks before crack initiation is 3.0E+06, the failure probability is 11%.

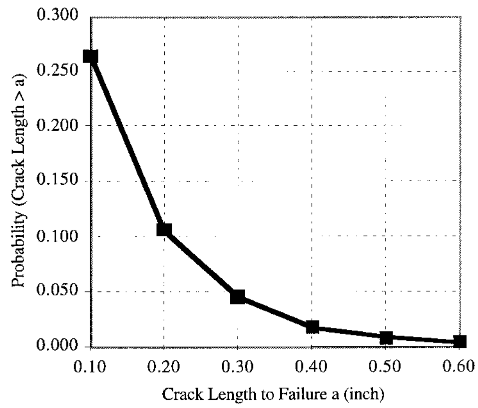

Fig. 15 CDF of failure of crack-propagation life.

Because the crack starts at node 1216, the probabilistic crack-propagation-life prediction is carried out at the same node. In addition to the eight tolerance random variables listed in Table 1, the material random variables and their statistical values are listed in Table 2. The AMV+ method in the fast probable integration,[34] is used to calculate the reliability. The CDF of the crack-propagation life (crack length to failure) at node 1216 is shown in Fig. 15 with a required number of service blocks 5.0E+06. The horizontal axis in Fig. 15 is the critical crack length to failure, and the vertical axis is the failure probability in which the crack-propagation length exceeds the critical length, or a critical crack length for a required failure probability. For example, if a 99.5% reliability (0.5 failure probability) is required, the critical crack length is about 0.5 in. It means that the probability of the crack growing to 0.5 in. from an initial length of 0.025 in. after 5.0E+06 service blocks is 0.5%.

Conclusions

An efficient reliability analysis method for the durability of structural components subjected to external and inertial loads with time-dependent variable amplitudes is presented. The proposed method is demonstrated to be effective for industrial-type applications, such as the tracked-vehicle roadarm. The proposed method has been employed to support a mixed design approach for probabilistic durability. The proposed method also is being extended to low-frequency flexible structures, such as vehicle body structures, thermal-induced fatigue for vehicle powertrain components, and system-level reliability.

Acknowledgment

Research was supported by the Automotive Research Center sponsored by the U.S. Army Tank and Automotive Command Center.

References

[1]Madsen, H. O., "Fatigue Reliability of Marine Structures," *Stochastic Approach to Fatigue*, edited by K. Sobczk, Springer–Verlag, New York, 1993.

[2]Bannantine, J. A., Comer, J. J., and Handrock, J. L., *Fundamentals of Metal Fatigue Analysis*, Prentice–Hall, Englewood Cliffs, NJ, 1990.

[3]Millwater, H., Wu, Y.-T., Trong, Y., Riha, D., and Leung, C., "Recent Developments of the NESSUS Probabilistic Structural Analysis Computer Program," AIAA Paper 92-2411, 1992.

[4]Besterfield, G. H., Liu, W. K., Lawrence, M. A., and Belytschko, T., "Fatigue Crack Growth Reliability by Probabilistic Finite Elements," *Computer Methods in Applied Mechanics and Engineering*, Vol. 86, 1991, pp. 297–320.

[5]Wu, Y. T., and Wirsching, P. H., "Advanced Reliability Method for Fatigue Analysis," *Journal of Engineering Mechanics*, Vol. 110, 1984, pp. 536–563.

[6]Hasofer, A. M., and Lind, N. C., "Exact and Invariant Second-Moment Code Format," *Journal of the Engineering Mechanics Division, ASCE*, Vol. 100, 1974, pp. 111–121.

[7]Wu, Y.-T., Millwater, H., and Cruse, T. A., "Advanced Probabilistic Structural Analysis Method for Implicit Performance Functions," *AIAA Journal*, Vol. 28, No. 9, 1990, pp. 1663–1669.

[8]Wang, L. P., and Grandhi, R. V., "Efficient Safety Index Calculation for Structural Reliability Analysis," *Computers and Structures*, Vol. 52, No. 1, 1994, pp. 103–111.

[9]Wang, L. P., and Grandhi, R. V., "Intervening Variables and Constraint Approximations in Safety Index and Failure Probability Calculations," *Structural Optimization*, Vol. 10, No. 1, 1995, pp. 2–8.

[10]*Fatigue Crack Growth Computer Program NASA/FLAGRO*, Ver. 2.0, NASA Johnson Space Center, Houston, TX, Aug. 1994.

[11]Chang, K. H., Yu, X., and Choi, K. K., "Design Sensitivity Analysis and Optimization (DSO)—Structural Reliability Analysis," *First World Congress of Structural and Multidisciplinary Optimization* (Goslar, Lower Saxony, Germany), WCSMO-1, Redwood Books, Trowbridge, England, UK, 1996, pp. 889–894.

[12]Choi, K. K., and Haug, E. J., "Shape Design Sensitivity Analysis of Elastic Soilds," *Journal of Structural Mechanics*, Vol. 11, No. 2, 1983, pp. 231–269.

[13]Haug, E. J., Choi, K. K., and Komkov, V., *Design Sensitivity Analysis of Structural Systems*, Academic, New York, 1986.

[14]Rosenblatt, M., "Remarks on a Multivariate Transformation," *Annals of Mathematical Statistics*, Vol. 23, 1952, pp. 470–472.

[15]Choi, K. K., Santos, J. L. T., and Frederick, M. C., "Implementation of Design Sensitivity Analysis with Existing Finite Element Codes," *Journal of Mechanisms, Transmissions, and Automation in Design*, Vol. 109, No. 3, 1987, pp. 385–391.

[16]Fadel, G. M., Riley, M. F., and Barthelemy, J. M., "Two-Point Exponential Approximation Method for Structural Optimization," *Journal of Structural Optimization*, Vol. 2, 1990, pp. 117–124.

[17]Barthelemy, J.-F. M., and Haftka, R. T., "Approximation Concepts for Optimum Structural Design—A Review," *Journal of Structural Optimization*, Vol. 5, No. 3, 1993, pp. 129–144.

[18]Sanders, J. R., and Tesar, D., "The Analytical and Experimental Evaluation of Vibration Oscillations in Realistically Proportioned Mechanisms," American Society of Mechanical Engineers, Paper 78-DE-1, 1978.

[19]Haug, E. J., *Computer-Aided Kinematics and Dynamics of Mechanical Systems: Basic Methods*, Vol. 1, Allyn and Bacon, Boston, 1989.

[20]*Concept Manual: Durability and Reliability Analysis Workspace*, Center for Computer-Aided Design, Univ. of Iowa, Iowa City, IA, 1994.

[21]Chang, K. H., Yu, X., and Choi, K. K., "Shape Design Sensitivity Analysis and Optimization for Structural Durability," *International Journal of Numerical Methods in Engineering*, Vol. 40, 1997, pp. 1719–1743.

[22]*ANSYS User's Manuals*, Ver. 5.0, Vols. 1–4, Swanson Analysis Systems, Inc., Houston, PA, 1992.

[23]Bannantine, J. A., Comer, J. J., and Handrock, J. L., *Fundamentals of Metal Fatigue Analysis*, Prentice–Hall, 1990.

[24]Tipton, S. M., "Fatigue Behavior Under Multiaxial Loading in the Presence of a Notch: Methodologies for the Prediction of Life to Crack Initiation and Life Spent in Crack Propagation," Ph.D. Thesis, Stanford Univ., Stanford, CA, 1984.

[25]"Case of the ASME Boiler and Pressure Vessel Code," Case N-47-12 (1592-2), American Society of Mechanical Engineers, New York, 1977.

[26]Chu, C. C., Conle, F. A., and Bonnen, J. J. F., "Multiaxial Stress-Strain Modeling and Fatigue Life Prediction of SAE Axle Shafts," *Advances in Multiaxial Fatigue*, ASTM STP 1191, American Society for Testing and Materials, Philadelphia, 1993, pp. 37–54.

[27]Gonyea, D. C., "Method for Low-Cycle Fatigue Design Including Biaxial Stress and Notch Effects," *Fatigue at Elevated Temperatures*, ASTM STP 520, American Society for Testing and Materials, Philadelphia, 1973, pp. 678–687.

[28]Rice, R. (ed.), *SAE Design Handbook*, Society of Automotive Engineers, Warrendale, PA, 1988, pp. 124, 125.

[29]Baek, W. K., and Stephenv, R. I., "Computational Life Prediction Methodology for Mechanical Systems Using Dynamic Simulation, Finite Element Analysis, and Fatigue Life Prediction Methods," Center for Computer-Aided Design, TR R-71, Univ. of Iowa, Iowa City, IA, 1990.

[30]Newman, J. C., Jr., "A Crack Opening Stress Equation for Fatigue Crack Growth," *International Journal of Fracture*, Vol. 24, No. 3, 1984, pp. R131–R135.

[31]Saouma, V. E., and Zatz, I. J., "An Automated Finite Element Procedure for Fatigue Crack Propagation Analysis," *Engineering Fracture Mechanics*, Vol. 20, No. 2, 1984, pp. 321–333.

[32]Choi, K. K., and Chang, K. H., "A Study on Velocity Field Computation for Shape Design Optimization," *Journal of Finite Elements in Analysis and Design*, Vol. 15, 1994, pp. 317–341.

[33]*DADS User's Manual*, Rev. 7.5, CADSI Inc., Oakdale, IA, 1994.

[34]Liu, P.-L., and Der Kiurehian, A., "Optimization Algorithms for Structural Reliability," *Structural Safety*, Vol. 9, No. 3, 1991, pp. 161–177.

G. A. Kardomateas
Associate Editor